Multi-omics analysis reveals psoralen to suppresses renal cell carcinoma through the PI3K/AKT pathway

DI CHEN[1,2*], TINGTING CHEN[2*], YURU YANG[2] and ANDONG WANG[2]

[1]Scientific Research Department, Ningbo Municipal Hospital of Traditional Chinese Medicine and Affiliated Hospital of Zhejiang Chinese Medical University, Ningbo, Zhejiang 315010, P.R. China; [2]School of Pharmacy, Nantong University, Nantong, Jiangsu 226001, P.R. China

Received August 22, 2025; Accepted February 19, 2026

DOI: 10.3892/mco.2026.2942

Abstract. Psoralen (PSO) is the active component of *Trigonostemon xyphophyllorides* (TX) and exhibits therapeutic potential against renal cell carcinoma (RCC). Despite this, there is a lack of research investigating the therapeutic efficacy of PSO specifically on RCC. In the present study, an integrated multi-omics strategy was employed to systematically evaluate the anti-RCC effects of PSO. PSO was subjected to network pharmacology analysis, identifying 78 RCC-related target genes. Pathway enrichment analysis suggested the involvement of the PI3K/AKT signaling pathway as a key regulatory mechanism. Molecular docking analysis and molecular dynamics simulations indicated a strong binding affinity and enhanced structural stability of the bound complexes between PIK3CA (PDB ID: 9B4T) and PSO. *In vitro* experiments demonstrated a potent antiproliferative effect of PSO on multiple RCC cell lines, with the strongest inhibition observed in ACHN cells (IC_{50} = 1.74±0.90 μM), By contrast, minimal cytotoxicity was observed towards the non-cancerous renal epithelial cell line HK-2 at concentrations ≤8 μM. Furthermore, PSO treatment resulted in the significant downregulation of the PI3K-AKT signaling pathway-related genes, which was supported by results from transcriptomic analysis identifying 593 differentially expressed genes. The present findings offer quantitative and mechanistic evidence supporting the clinical utilization of TX in the treatment of RCC, thereby advancing its further research and development.

Correspondence to: Professor Andong Wang, School of Pharmacy, Nantong University, 9 Seyuan Road, Nantong, Jiangsu 226001, P.R. China
E-mail: wangandong19891220@163.com

Professor Di Chen, Scientific Research Department, Ningbo Municipal Hospital of Traditional Chinese Medicine and Affiliated Hospital of Zhejiang Chinese Medical University, 819 Liyuan North Road, Haishu, Ningbo, Zhejiang 315010, P.R. China
E-mail: zjnbcd@163.com

*Contributed equally

Abbreviations: BC, Betweenness centrality; BP, biological process; CC, cellular component; MF, molecular function; PSO, psoralen; RCC, renal cell carcinoma; RG, radius of gyration; RMSD, root mean square deviation; RMSF, root mean square fluctuation; TX, *Trigonostemon xyphophyllorides*

Key words: PSO, TX, RCC, computer simulation, PI3K-AKT signaling pathway

Introduction

Renal cell carcinoma (RCC) is a prevalent and highly lethal cancer affecting the genitourinary system. It is particularly prevalent in men, with a mortality rate ranging from 30-40%. Risk factors for RCC include sex, obesity, hypertension, smoking and chronic kidney disease (1,2). Treatment typically involves surgical intervention, namely either total or partial nephrectomy, but such radical procedures can significantly impact the quality of life of patients. Complementary to surgery, targeted pharmacotherapies are pivotal in managing RCC (3). Nevertheless, the high cost associated with these advanced therapies limits their widespread adoption amongst patients with RCC, underscoring the critical need for cost-effective treatment alternatives (4,5).

Traditional Chinese medicines have been garnering increasing global attention due to their extensive historical use and notable efficacy. With the advancement of modern pharmacology and systems biology approaches, increasing efforts have been devoted to elucidating the molecular mechanisms underlying their therapeutic effects. Understanding of their mechanisms of action has advanced as a result of progress in modern pharmacological techniques (6).

Plants of the genus *Trigonostemon*, belonging to the Euphorbiaceae family, are prevalent in tropical and temperate regions. They have a long history of medicinal use (7,8). In particular, *Trigonostemon xyphophyllorides* (Croizat) L. K. Dai and T. L. Wu (TX) root is a local herb that is traditionally used in Thailand for treating food poisoning and snake bites. In China, the bark of this herb has been utilized to alleviate asthma symptoms (9). Modern pharmacological studies have identified TX to possess antiviral, antitumor, antibacterial, anti-inflammatory and insecticidal properties (10-13). Previous *in vitro* experiments have demonstrated that the coumarin compound psoralen (PSO, PubChem CID 6199), which is found in TX, exhibits potent antitumor effects, suggesting its

potential as a natural anticancer agent (14,15). Despite accumulating evidence supporting the antitumor activity of PSO, its therapeutic efficacy and more importantly its underlying molecular mechanisms in RCC regulation remain poorly understood. The signaling pathways and key molecular targets through which PSO exerts anti-RCC effects remain to be fully elucidated. Therefore, the aim of the present study was to systematically investigate the anti-RCC effects of PSO using an integrated multi-omics strategy, combining network pharmacology, molecular docking, molecular dynamics simulation, transcriptomic analysis and experimental validation. The present study seeks to offer both experimental and mechanistic evidence supporting the clinical utilization of TX in treating RCC, thereby advancing its research and development.

Materials and methods

Plant sources. The TX branches utilized in the present were obtained from Haikou (China) and authenticated as TX by Professor Guangtong Chen from the Department of Pharmacy, of Nantong University. A voucher specimen (no. 2023026) has been archived at the Herbarium Center, School of Pharmacy of Nantong University.

PSO extraction and structure determination. The branches of TX were subjected to three rounds of extraction with 95% ethanol under reflux conditions for 2 h each. The herbal extract underwent purification through sequential passage through silica gel column chromatography, gel column chromatography and high-performance liquid chromatography [JAI LC9103 Recycling preparative HPLC (Japan Analytical Industries), JAIGEL-ODS-AP-P column and JAIGEL-GS310 column using a JAI refractive index detector and a JAI UV-3702 detector with MultiChro 2000 workstation, 50 μl, MeOH-H_2O (55:45), 10 ml/min] to isolate pure PSO (11.2 mg). The identity of PSO was confirmed by comparison of the monomer with literature data using ^{1}H nuclear magnetic resonance (NMR) and ^{13}C NMR analyses (16,17).

Target gene prediction. Potential gene targets of PSO were predicted using the Swiss Target Prediction database (https://www.swisstargetprediction.ch/). To identify target genes associated with RCC, databases, including OMIM (https://www.omim.org/), DrugBank (https://go.drugbank.com/), DisGeNet (https://disgenet.com/), Genecards (https://www.genecards.org/) and Therapeutic Target Database (TTD; https://ttd.idrblab.cn/), were queried. Compound and disease-related gene sets were compiled by merging and removing duplicates. The overlapping genes were analyzed to propose potential compound target genes for RCC. These databases were selected due to their complementary strengths in covering genetic associations, curated therapeutic targets and disease relevance, which are widely used in network pharmacology studies to improve target prediction reliability.

Protein-protein interaction (PPI) network construction. The potential target genes were inputted into the STRING database https://string-db.org/ at a confidence level of 0.7 and subsequently imported into Cytoscape 3.10.2 software (https://cytoscape.org/). Utilizing the metrics of Degree, Betweenness Centrality (BC) and Closeness Centrality (CC), the PPIs were visualized. A positive correlation between these metrics and the therapeutic efficacy of target genes on RCC was observed, indicating a stronger influence of genes with higher values on the therapeutic potential.

Kyoto Encyclopedia of Genes and Genomes (KEGG) and Gene Ontology (GO) analysis. The high-impact target genes were inputted into the Sandbox database (http://www.sangerbox.com/home.html), with human subjects selected, a minimum overlap value of 3, a significance threshold of $P<0.05$, and a minimum enrichment threshold of 1.5. Subsequently, KEGG pathway enrichment and GO function analyses were conducted, where the top-ranked KEGG and GO data were summarized and visualized through histogram analysis (18).

Molecular docking. The PDB file of the high-impact target gene was downloaded from the database (https://www.rcsb.org/) and Discovery Studio (v 1.21) was used to visualize its ligand and water molecule configuration. Subsequently, ChemDraw 3D software (2020) was used to open the compound structure and execute energy minimization to produce the MOL2 file format. AutoDock software (1.5.7) was then used for docking the compound and high-impact target genes to assess the binding free energy, where a greater absolute value signifies a stronger interaction (18,19).

Molecular dynamics simulations. Following molecular docking, the top-performing complexes were chosen for kinetic simulation and visualization. Protein FASTA sequences were retrieved from the RCSB PDB and modeled using Swiss-Model (https://swissmodel.expasy.org/). The protein structure was refined by filling in missing data and adding hydrogen atoms via Protein Plus (https://g6altair.sci.hokudai.ac.jp/g6/service/pocasa/). Topology files were generated using ACPYPE (2022.1.3) for molecular dynamics simulations. GROMACS software (2024.2) was employed with the AMBER 14SB force field and TIP3P water model, ensuring a minimum distance of 1.2 nm from the protein edges to the box boundaries.

Cell viability assay. The cell lines 769-P, 786-0, ACHN and HK-2 were procured from the National Collection of Authenticated Cell Cultures. Cells underwent STR certification and were stored in a humidified environment at 37˚C with 5% CO_2. The cells were treated with varying concentrations of PSO (0, 2, 4, 8, 16 μM) to induce stabilization, followed by assessment of cell viability using the Cell Counting Kit-8 (CCK-8) assay post drug administration. Cells in the logarithmic growth phase ($5x10^4$ cells/ml) were seeded into a 96-well plate at 100 μl per well. Subsequently, 10 μl of test substances at varying concentrations were added to each well for a 24-h treatment period. Following this, 10 μl of CCK-8 solution was introduced to each well, and the plate was returned to the incubator for an additional 2 h. Absorbance (OD value) was then measured at 450 nm using a microplate reader, and cell survival rates at different concentrations, along with the IC_{50} value, were calculated.

Transcriptomic analysis. Tumor tissues underwent standard preprocessing procedures to prepare them for transcriptome sequencing in subsequent investigations. RNA quality in skin samples was assessed using an Agilent 2100 bioanalyzer. Ribosomal RNA (rRNA) removal, library construction, and Illumina sequencing were conducted by Beijing Novogene Bioinformatics Technology Co., Ltd. Bowtie software (v2.5.0) was utilized to eliminate rRNA sequences from the raw sequencing reads, using the mouse-derived rRNA reference sequence as the index. The mem algorithm of BWA software (v0.7.17-r1188) aligned the filtered clean reads with the mouse reference genome (Mus Musculus (GRCm38/mm10)). SAM format files were converted to BAM format using Samtools software (v1.8), followed by sorting and indexing. FeatureCounts software (v2.0.1) counted the uniquely aligned reads to determine the raw expression levels of each gene. Differentially expressed genes were then identified using R language, following the standard differential expression analysis workflow. For small sample sizes, DESeq2 (v1.34.0) was employed, while the Wilcoxon rank-sum test was used for larger sample sizes. Genes were considered differentially expressed if they had a corrected P-value <1.0. Initially, reads exhibiting low-quality base ratios exceeding 40%, comprising over 1% unknown bases, and showing contamination from adapter sequences were eliminated using SOAPnuke (2024.2). DESeq2 was employed to pinpoint differentially expressed genes with Fold Change (FC) >2 or 1.0 and P<0.05.

Statistical analysis. Data analysis was conducted using SPSS 22.0 software (IBM Corp.). Mean values with standard deviations were utilized to represent data variability. Group comparisons were performed using one-way paired t-tests. P<0.05 was considered to indicate a statistically significant difference.

Results

Structural determination. The structure of the compound was elucidated using various chromatographic techniques, where its NMR data are presented as follows: ^{1}H NMR (400 MHz, DMSO-*d*6) δ_H 8.17 (d, *J*=9.6 Hz, 1H, H-4), 8.11 (d, *J*=2.3 Hz, 1H, H-2'), 8.00 (s, 1H, H-6), 7.72 (s, 1H, H-8), 7.10 (dd, *J*=2.3, 0.9 Hz, 1H, H-3'), 6.43 (d, *J*=9.6 Hz, 1H, H-3) (Fig. S1). ^{13}C NMR (100 MHz, DMSO-*d*6) δ_C 160.2(C-2), 155.7(C-7), 151.5(C-9), 147.9(C-2'), 145.0(C-4), 124.6(C-6), 120.7(C-5), 115.4(C-10), 114.1(C-3), 106.8(C-3'), 99.3(C-8) (Fig. S2). A literature review confirmed the compound as PSO (20), a natural furanocoumarin initially isolated from *Psoralea corylifolia*.

Target gene prediction. Prediction of PSO using the Swiss Target Prediction database identified 162 potentially relevant genes. Searching for genes related to RCC yielded 3,687 genes from GeneCards, 179 genes from DisGeNET, 200 genes from OMIM, 30 genes from DrugBank and 54 genes from the TTD database. After removing duplicates, a total of 3,923 genes were predicted. The intersection of these datasets revealed 78 target genes associated with RCC (Fig. S3).

PPI network analysis. A PPI network diagram was constructed based on the 78 predicted target genes, where the top 20 genes were ranked according to Degree, BC and CC metrics. The results, presented in Table I, revealed that the top five genes were ESR1 (Degree=41, BC=0.1679 and CC=0.6788), HSP90AB1 (Degree=38, BC=0.118611 and CC=0.6666), NFKB1 (Degree=38, BC=0.1186 and CC=0.6666), NFKB1 (Degree=38, BC=0.0552 and CC=0.6491) and STAT1 (Degree=31, BC=0.0338 and CC=0.5967).

Table I. Gene names, degree value, betweenness centrality and closeness centrality of key targets.

Gene name	Betweenness centrality	Closeness centrality	Degree
ESR1	0.167942	0.678899	41
HSP90AB1	0.118611	0.666667	38
NFKB1	0.055249	0.649123	38
STAT1	0.033857	0.596774	31
GSK3B	0.052042	0.611570	31
TLR4	0.055006	0.606557	31
PARP1	0.043182	0.587302	28
PIK3CA	0.046844	0.573643	27
RELA	0.015787	0.578125	26
ICAM1	0.028730	0.564885	24
JAK2	0.028848	0.544118	23
NFE2L2	0.015432	0.564885	23
NFKBIA	0.018060	0.560606	22
MAPK14	0.043738	0.544118	22
PGR	0.013787	0.540146	21
RPS6KB1	0.006633	0.536232	20
AR	0.007943	0.540146	20
PPARA	0.041333	0.536232	19
ESR2	0.034383	0.532374	17
HDAC2	0.018560	0.503401	16

KEGG and GO analysis. After analyzing 78 potential target genes using KEGG pathway enrichment in the database, a total of 131 signaling pathways were identified. The top 10 enriched KEGG pathways included 'Pathways in cancer', 'Metabolic pathways', 'Kaposi sarcoma-associated herpesvirus infection', 'Hepatitis B', 'Chemokine signaling pathway', 'PI3K-Akt signaling pathway', 'Human cytomegalovirus infection', 'Prolactin signaling pathway', 'Epstein-Barr virus infection' and 'cAMP signaling pathway' (Fig. S4).

The 78 potential target genes underwent analysis using the GO Functional Enrichment Database, yielding 267 molecular function (MF) results, 98 cellular component (CC) results, and 2,134 biological process (BP) results. The top 5 MF results included 'enzyme binding', 'catalytic activity', 'protein kinase activity', 'phosphotransferase activity' and 'alcohol group as acceptor'. The top 5 CC results consisted of 'cytosol', 'cell surface', 'whole membrane', 'nucleoplasm' and 'plasma membrane part'. The top 5 BP results were 'response to organic substance', 'response to chemical', 'response to oxygen-containing compound', 'cellular response to chemical stimulus' and 'regulation of biological quality' (Fig. S5).

Molecular docking. The protein genes with high degree values within the PI3K/Akt/mTOR signaling pathway, crucial in the therapeutic process of RCC, were chosen for molecular docking simulations with PSO to assess their binding capabilities. Selected proteins included heat shock protein (HSP)90AB1 (PDB ID: 5UC4), NFKB1 (PDB ID: 1U3Y), glycogen synthase kinase (GSK)3B (PDB ID: 6AE3), toll-like receptor (TLR)4 (PDB ID: 5UCA), PIK3CA (PDB ID: 9B4T), RELA (PDB ID: 1VJ7), Janus kinase (JAK)1 (PDB ID: 6GGH) and JAK2 (PDB ID: 7F7W). The docking results revealed binding energies of -6.14 kcal/mol with 5UC4, -5.226 kcal/mol with 1U3Y, -7.33 kcal/mol with 6AE3, -0.198 kcal/mol with 5UCA, -7.47 kcal/mol with 9B4T, -7.07 kcal/mol with 1VJ7, -6.514 kcal/mol with 6GGH and -6.18 kcal/mol with 7F7W. The complex with the highest absolute docking binding energies was chosen for in-depth molecular docking analysis (Fig. 1A).

Molecular dynamics simulations. PSO with 9B4T kinetic simulation preprocessing was employed, modeling the system with dimensions of 13.711x13.711x13.711 nm, each angle at 90.00˚ and a volume of 2,577.47 nm^3. The final configuration consisted of 254,810 atoms distributed over 80,730 residues, with a solvent density of 1,001.99 g/l and 79,781 solvent molecules. Sodium ions were introduced to maintain charge balance, with a salt solution concentration of 0.15 mol/l to mimic physiological conditions. Electrostatic interactions were computed using Particle-mesh Ewald for energy minimization over 50,000 steps. The system was simulated in canonical ensemble and isothermal-isobaric ensemble states at 310 K and 1 bar pressure. Molecular dynamics simulations were conducted for 250 ns under these conditions, with a non-bonded interaction cutoff of 10 Å. The simulation results were evaluated based on root mean square deviation (RMSD), root mean square fluctuation (RMSF), radius of gyration (RG) and hydrogen bond energy.

The RMSD of the PSO/9B4T complex was comparable to but slightly lower compared with that of the unbound protein, indicating reduced structural deviation and enhanced stability (Fig. 1B). PSO/9B4T maintains lower and less fluctuating RMSF values, indicating higher structural stability and suggesting a more stable structure for the PSO/9B4T complex (Fig. 1C). The RG of the PSO/9B4T complex fluctuated within a narrow range (3.11-3.16 nm), with an average value of ~3.13 nm, indicating a compact and stable complex throughout the simulation (Fig. 1D). In the PSO/9B4T complex, the majority of hydrogen bonds were concentrated between 1 and 2, indicating a relatively stable state of low-frequency hydrogen bonding throughout most time points (Fig. 1E). Quantitative analysis showed that the average RMSD of the PSO-PIK3CA complex was lower compared with that of the unbound protein during the equilibrium phase, indicating enhanced structural stability. The average RG of the complex remained stable at ~3.13 nm, with smaller fluctuations compared with the apo protein, further supporting the formation of a stable complex.

Cell viability test results. Initially, the toxic impact of PSO was assessed on normal cells. Various doses of PSO were administered to normal renal epithelial cells (HK-2), where cell viability was assessed using the CCK-8 assay. The results indicated that PSO exhibited no significant toxicity towards HK-2 cells within the 0-8 μM range, instead demonstrating slight cytotoxicity at a higher concentration of 16 μM. PSO treatment resulted in the significantly decreased cellular viability of 769-P and 786-0 cells (IC_{50} values of 6.02±0.88 and 6.26±0.96 μM, respectively). Furthermore, PSO significantly decreased the cellular viability of ACHN cells, with an IC_{50} of 1.74±0.90 μM (Fig. 1F).

Transcriptomics results. Transcriptomics analysis was utilized to comprehensively assess genetic changes in tumor cells before and after drug administration. Comparison of gene expression differences between MOD and PSO groups through volcano and heat map analyses (Fig. 2A and B) revealed 112 upregulated genes and 481 downregulated genes. Due to the substantial number of differential genes, PPI analysis was conducted using the STRING database to identify potential target genes. Selection criteria included Degree ≥7, BC ≥0.0019 and CC ≥0.2976. Ultimately, 100 significant target genes were identified and visualized based on their degree values (Fig. 2C). KEGG pathway enrichment analysis of these target genes identified 48 highly enriched pathways, with the top 20 pathways including 'cytokine-cytokine receptor interaction', 'chemokine signaling pathway', 'tuberculosis' and others (Fig. 2D). GO functional analysis visualized the top 10 results for MF, CC and BP (Fig. 2E). Transcriptomics pathway enrichment results indicated significant downregulation of OSM, FGF23, FGF5 and other genes in the PI3K/Akt pathway ($P<0.001$), suggesting differential changes at the transcriptome level and supporting the pathway's role in the therapeutic process.

Discussion

PSO is a bioactive furanocoumarin that can be isolated from TX and has been reported to exhibit broad antitumor activities in multiple cancer types. Previous studies have demonstrated that PSO can suppress tumor cell proliferation by inducing apoptosis in hepatocellular carcinoma, breast cancer, gastric cancer and osteosarcoma through various mechanisms, including DNA damage, inhibition of DNA polymerase and topoisomerase II, endoplasmic reticulum stress and regulation of microRNA-associated signaling pathways (17-19). However, these studies primarily focused on tumor types outside the renal system, where the molecular mechanisms underlying PSO activity in RCC remained largely unexplored.

In the present study, the anti-RCC effects of PSO were systematically investigated using an integrated multi-omics strategy. Compared with previous studies in other cancer models, the present findings highlight a distinct but convergent mechanism in RCC, characterized by suppression of the PI3K/AKT signaling pathway (20). Network pharmacology and transcriptomic analyses consistently identified PI3K/AKT-related genes as central nodes in PSO-mediated regulation, whilst molecular docking and molecular dynamics simulations further supported a stable interaction between PSO and PIK3CA.

The PI3K/AKT signaling pathway is a well-established driver of RCC progression, regulating cell proliferation, survival, metabolism and therapeutic resistance. Natural

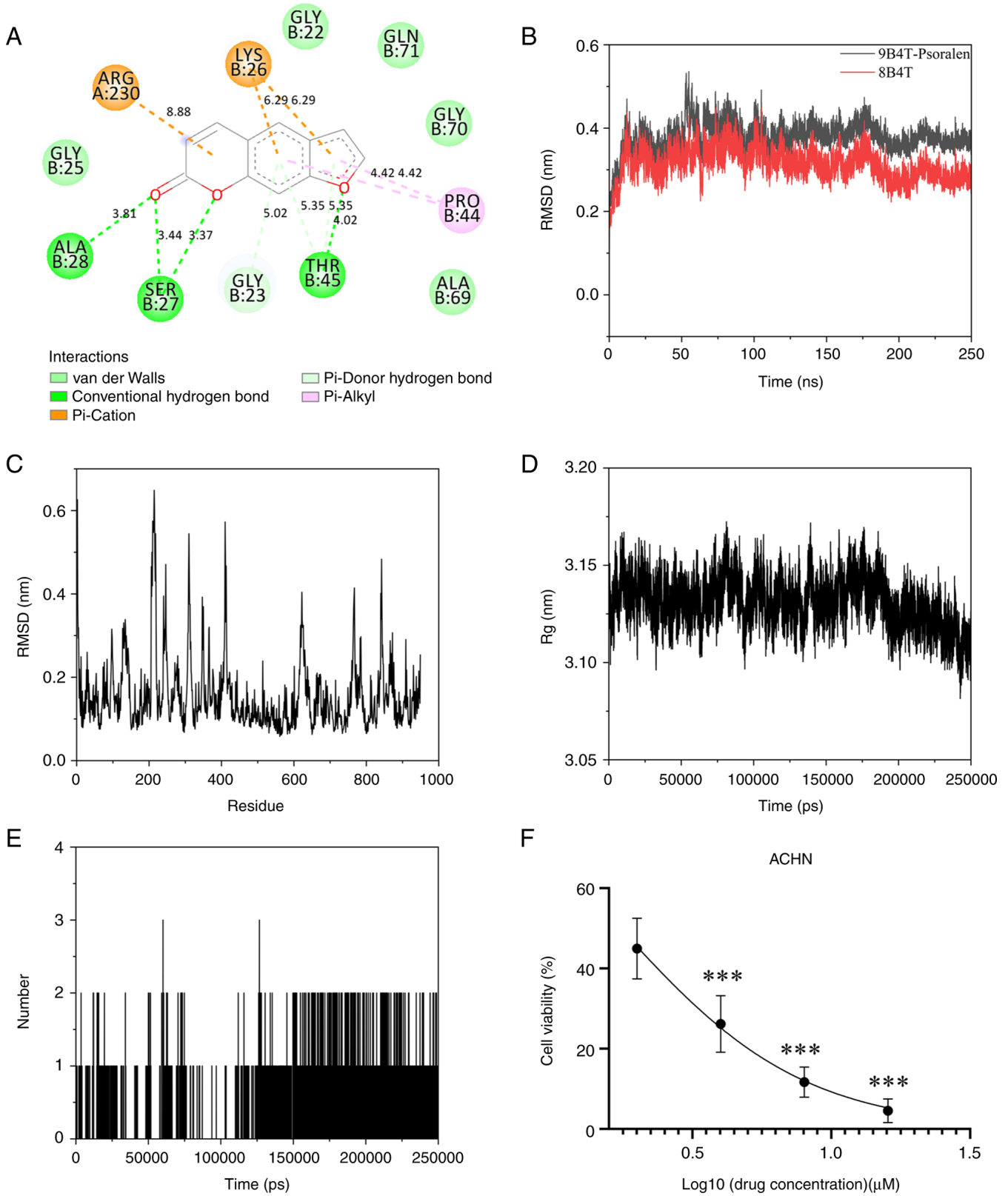

Figure 1. (A) Molecular docking diagram. (B) RMSD values with the red curve denoting the original protein and the black curve denoting the complex. (C) RMSF values. (D) RG values. (E) Hydrogen bond energy values. (F) Cell viability tests conducted on ACHN cells. RMSD, root mean square deviation; RMSF, root mean square fluctuation; RG, radius of gyration. ***P<0.001, compared with 0 μM PSO.

products targeting this pathway have shown promise in RCC treatment. *Hemsleya amabilis* Diels extract has been shown to induce G2/M cell cycle arrest and apoptosis in RCC models through the PI3K/AKT pathway inhibition, effects that were reversed by PI3K inhibition (21). Similarly, gypenosides from *Gynostemma pentaphyllum* was observed to suppress RCC cell proliferation and promoted apoptosis by downregulating PI3K, AKT and mTOR

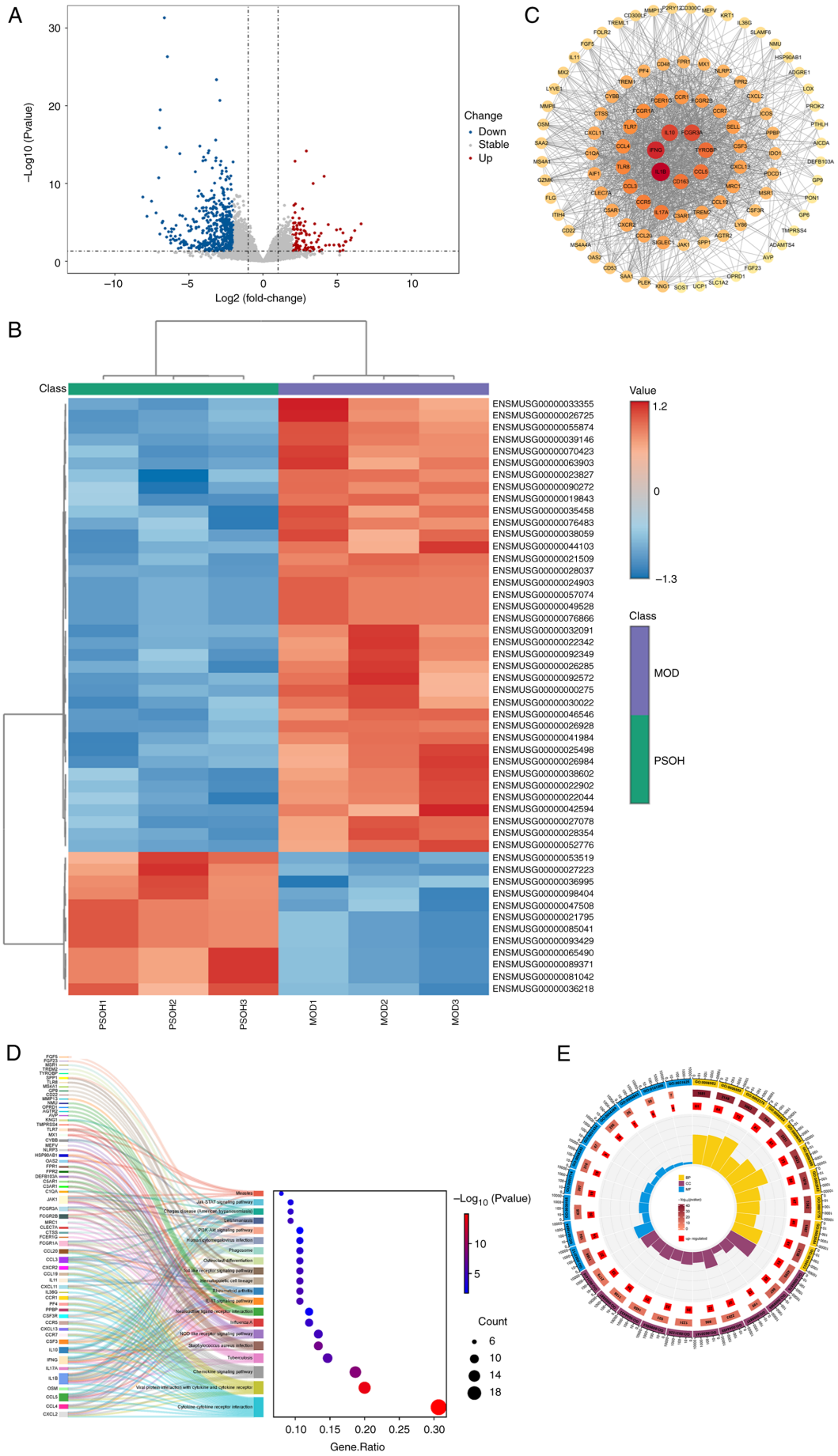

Figure 2. (A) Volcano map depicting transcriptomics data. (B) Heat map analysis of transcriptomics. (C) Visualization of the top 100 ranked genes, darker colors indicate higher degree values. (D) Kyoto Encyclopedia of Genes and Genomes pathway enrichment map. (E) Gene Ontology functional analysis map (n=3).

expression (22). Consistent with these studies, the results of the present study demonstrated that PSO significantly downregulates PI3K/AKT pathway-related genes and inhibits RCC cell proliferation, positioning PSO as a natural PI3K/AKT-modulating agent in RCC.

Based on these findings, a schematic mechanism was proposed in which PSO interacts with PIK3CA, leading to the suppression of PI3K/AKT signaling, disruption of downstream survival and proliferative signals, ultimately inhibiting RCC tumor growth. This integrated mechanism bridges computational predictions with experimental validation and provides a coherent framework for understanding anti-RCC activity of PSO.

In summary, the present study systematically elucidated the anti-RCC effects of PSO derived from TX using an integrated multi-omics approach. The present findings demonstrated that PSO exerts significant antiproliferative effects on RCC cells primarily through suppression of the PI3K/AKT signaling pathway, supported by network pharmacology, molecular docking, molecular dynamics simulations, transcriptomics and *in vitro* validation.

These results not only extend the antitumor spectrum of PSO to RCC but also highlight its potential as a natural PI3K/AKT pathway modulator. Given the clinical importance of PI3K/AKT signaling in RCC progression and therapeutic resistance, PSO may represent a promising lead compound for the development of cost-effective and mechanism-based therapeutic strategies for RCC. Further preclinical and clinical investigations are warranted to explore its translational potential.

Acknowledgements

Not applicable.

Funding

The present study was supported by the National Natural Science Foundation of China (grant no. 32200314), the Ningbo Health Technology Project (grant no. 2022Y18) and the Research Project of Zhejiang Chinese Medical University (grant no. 2022FSYYZQ19) and the Ningbo Natural Science Foundation (grant no. 2024J261).

Availability of data and materials

The data generated in the present study may be requested from the corresponding author.

Authors' contributions

DC and TC made substantial contributions to conception and design; acquisition, analysis and interpretation of data and were involved in drafting or revising the manuscript critically for important intellectual content. TC and AW confirm the authenticity of all the raw data and provided final approval for publication. DC, TC, YY and AW participated sufficiently in the work to take public responsibility for appropriate portions of the content and agreed to be accountable for all aspects of the work in ensuring that questions related to the accuracy or integrity of any part of the work are appropriately investigated and resolved. All authors read and approved the final version of the manuscript.

Ethics approval and consent to participate

Not applicable.

Patient consent for publication

Not applicable.

Competing interests

The authors declare that they have no competing interests.

References

1. Chen YW, Wang L, Panian J, Dhanji S, Derweesh I, Rose B, Bagrodia A and McKay RR: Treatment landscape of renal cell carcinoma. Curr Treat Options Oncol 24: 1889-1916, 2023.
2. Nezami BG and MacLennan GT: Clear cell renal cell carcinoma: A comprehensive review of its histopathology, genetics, and differential diagnosis. Int J Surg Pathol 33: 265-280, 2025.
3. Wolf MM, Kimryn Rathmell W and Beckermann KE: Modeling clear cell renal cell carcinoma and therapeutic implications. Oncogene 39: 3413-3426, 2020.
4. Siva S, Bressel M, Sidhom M, Sridharan S, Vanneste BGL, Davey R, Montgomery R, Ruben J, Foroudi F, Higgs B, *et al*: Stereotactic ablative body radiotherapy for primary kidney cancer (TROG 15.03 FASTRACK II): A non-randomised phase 2 trial. Lancet Oncol 25: 308-316, 2024.
5. Wang L, Zong L, Cao D and Guan M: Unraveling the molecular mechanisms of PFOA in clear cell renal cell carcinoma through network toxicology and molecular docking strategies. Int J Surg 111: 4842-4853, 2025.
6. Jin J, Xie Y, Zhang JS, Wang JQ, Dai SJ, He WF, Li SY, Ashby CR Jr, Chen ZS and He Q: Sunitinib resistance in renal cell carcinoma: From molecular mechanisms to predictive biomarkers. Drug Resist Updat 67: 100929, 2023.
7. Song K, Li M, Yang Y, Zhang Z, Zhang J, Zhu Q, Liu J and Wang A: Trigonostemon species in south China: Insights on its chemical constituents towards pharmacological applications. J Ethnopharmacol 281: 114504, 2021.
8. Wang A, Yang Y, Chen T, He J, Ling B and Cheng X: Antiproliferative effects of *Trigonostemon xyphophyllorides* on renal cell carcinoma via the PI3K/AKT pathway. Front Pharmacol 16: 1594461, 2025.
9. Ban NK, Linh TM, Mai NC, Tai BH, Nhiem NX, Hoang NH and Kiem PV: New 3,4-seco-diterpene and coumarin derivative from the leaves of *Trigonostemon flavidus* Gagnep. Nat Prod Res 36: 3247-3254, 2022.
10. Ban NK, Truong LH, Tiep TV, Yen DTH, Doan VV, Nhiem NX, Seo Y, Namkung W, Kim SH, Tai BH and Kiem PV: Four new sucrose diesters of substituted truxinic acids from trigonostemon honbaensis with their anoctamin-1 inhibitory activity. Bioorg Chem 102: 104058, 2020.
11. Cho YR, Park K, Kang JS Byun HW, Oh JS, Seo DW and Ahn EK: *Trigonostemon reidioides* modulates endothelial cell proliferation, migration and tube formation via downregulation of the Akt signaling pathway. Oncol Lett 14: 4677-4683, 2017.
12. Liu YP, Hu S, Wen Q, Ma YL, Jiang ZH, Tang JY and Fu YH: Novel γ-lactone derivatives from trigonostemon heterophyllus with their potential antiproliferative activities. Bioorg Chem 79: 107-110, 2018.
13. Liu YP, Wen Q, Hu S, Ma YL, Jiang ZH, Tang JY and Fu YH: Structurally diverse diterpenoids from trigonostemon howii. Nat Prod Res 33: 1169-1174, 2019.
14. Sun B, Shen K, Zhao R, Li Y and Lin J: Clarithromycin attenuates airway epithelial-mesenchymal transition in ovalbumin-induced asthmatic mice through modulation of Kv1.3 channels and PI3K/Akt signaling. Int Immunopharmacol 139: 112624, 2024.

15. Chen S, Guo W, Liu H, Zheng J, Lu D, Sun J, Li C, Liu C, Wang Y, Huang Y, *et al*: Mechanistic study of cytochrome P450 enzyme-mediated cytotoxicity of psoralen and isopsoralen. Food Chem Toxicol 180: 114011, 2023.
16. Takeda J, Iwao Y, Karashima M, Yamamoto K and Ikeda Y: Structural evaluation of the choline and geranic acid/water complex by SAXS and NMR analyses. ACS Biomater Sci Eng 7: 595-604, 2021.
17. Wang Y, Zhang J, Xu S, Li J, Liu W, Jiang M and Bai G: Psoralen alleviates acute lung injury by covalently targeting Cys106 of HMGB1 in macrophages to inhibit inflammatory responses. Phytomedicine 142: 156807, 2025.
18. Li X, Miao F, Xin R, Tai Z, Pan H, Huang H, Yu J, Chen Z and Zhu Q: Combining network pharmacology, molecular docking, molecular dynamics simulation, and experimental verification to examine the efficacy and immunoregulation mechanism of FHB granules on vitiligo. Front Immunol 14: 1194823, 2023.
19. Lu S, Sun X, Zhou Z, Tang H, Xiao R, Lv Q, Wang B, Qu J, Yu J, Sun F, *et al*: Mechanism of bazhen decoction in the treatment of colorectal cancer based on network pharmacology, molecular docking, and experimental validation. Front Immunol 14: 1235575, 2023.
20. Chang J, Hu P, Zhang B, Liu Y, Cheng Y, Li L and Li L: Perilla seed oil alleviates high-fat-diet-induced hyperlipidemia by regulating fatty acid metabolism via the PI3K/Akt/NOS3 pathway. Foods 14: 4125, 2025.
21. Chen LM, Qian ST, Li ZQ, He MF and Li HJ: Psoralen and isopsoralen, two estrogen-like natural products from psoraleae fructus, induced cholestasis via activation of ERK1/2. Chem Res Toxicol 37: 804-813, 2024.
22. Shen Z, Gao X, Huang D, Xu X and Shen J: The potential of *gynostemma pentaphyllum* in the treatment of hyperlipidemia and its interaction with the LOX1-PI3K-AKT-eNOS pathway. Food Sci Nutr 12: 8000-8012, 2024.